PAPER

CrossMark
click for updates

Highly selective magnetic affinity purification of histidine-tagged proteins by Ni²⁺ carrying monodisperse composite microspheres†

Kouroush Salimi,[a] Duygu Deniz Usta,[bc] İlkay Koçer,[a] Eda Çelik[ad] and Ali Tuncel*[ae]

A magnetic sorbent with stable and superior magnetic behaviour was developed for His-tagged protein purification by immobilized metal affinity chromatography (IMAC). Magnetic, monodisperse and porous silica microspheres 6 μm in size, with bimodal pore size distribution including both mesoporous and macroporous compartments were synthesized as the base material by a staged-shape template hydrolysis & condensation protocol. The magnetic microspheres were functionalized with iminodiacetic acid (IDA) and Ni²⁺ ions were attached onto the microspheres by metal-chelate formation *via* carboxyl groups. The saturation magnetization and carboxyl content of IDA attached magnetic silica microspheres were determined as 22.1 emu g⁻¹ and 19 mmol IDA g⁻¹ microspheres, respectively. A superior magnetic response with respect to the currently available IMAC sorbents in the form of composite magnetic nanoparticles was obtained with the proposed sorbent. The magnetic sorbent was utilized for the isolation of His-tagged green fluorescent protein (GFP) from *E. coli* lysate in batch-fashion. The maximum equilibrium GFP adsorption was *ca.* 87 mg GFP per g sorbent. GFP was isolated with high selectivity (>95% purity) and isolation yields up to 68% by changing the magnetic sorbent concentration. The superior isolation performance of the sorbent was explained by the presence of a bimodal pore structure including both macropores facilitating the intraparticular diffusion of GFP, and the mesopores serving a large surface area for parking and adsorption of GFP into the microbeads.

1. Introduction

Recombinant protein technology plays an important role in the field of molecular biology for thoroughly understanding the structure and functions of proteins.[1–3] In protein engineering, hexa-histidine tag (6xHis-tag) is the most commonly used affinity tag for recombinant protein purification.[2–4] Among the various purification techniques, immobilized metal affinity chromatography (IMAC) and metal oxide affinity chromatography (MOAC) have been widely utilized for selective and reliable separation of His-tagged proteins based on the metal coordination interaction between histidine and transition metal ions.[5–8] In the case of IMAC sorbents, the divalent metal ions (Ni²⁺, Co²⁺, Cu²⁺ or Zn²⁺) have modest affinity constants

and higher ligand stability compared to biospecific affinity ligands.[6–9] These cations are immobilized to a solid support (sorbent) using iminodiacetic acid (IDA) or nitrilotriacetic acid (NTA) as metal chelating ligands. While the binding and elution conditions are usually optimized on a case-by-case basis, the trapped proteins are easily released by elution with imidazole or EDTA. Most of the conventional IMAC and MOAC based affinity methods have been reported as time consuming, having low reaction yields and complex pretreatments of the sorbents for protein separation.[10–12] The combination between magnetic composite microspheres and IMAC has been used as alternative sorbents, due to their high surface/volume ratio, high parking area as well as the stability of metal chelates.[13] Various kinds of immobilized magnetic composite microspheres with metal ions have been utilized for separation/purification of His-tagged proteins from various biological sources.[14–22] Furthermore, different nanomaterials based on Ni/NiO core/shell nanoparticles, Fe₃O₄/Au–ANTA–Co²⁺ nanoparticles, nickel silicate nanospheres, and Fe₃O₄@NiSiO₃ nanostructures are reported as MOAC based affinity adsorbents for His-tagged protein purification.[6,7,21,23] Recently, Li *et al.* reported a new separation material (SiO₂@IDA/MAPS nanoparticles) adopting epitope imprinting enhanced IMAC (EI-IMAC) to supply the affinity interaction, which showed good selectivity towards the His-tagged recombinant proteins from crude cell lysis.[24] Moreover,

ᵃ*Chemical Engineering Department, Hacettepe University, 06800, Ankara, Turkey. E-mail: atuncel@hacettepe.edu.tr; Fax: +90-312-299-21-24; Tel: +90-312-297-74-00*

ᵇ*Department of Medical Biology and Genetics, Gazi University, 06500, Ankara, Turkey*

ᶜ*Department of Medical Biology, İstanbul Medeniyet University, 34700, İstanbul, Turkey*

ᵈ*Institute of Science, Division of Bioengineering, Hacettepe University, 06800, Ankara, Turkey*

ᵉ*Division of Nanotechnology and Nanomedicine, Hacettepe University, 06800, Ankara, Turkey*

† Electronic supplementary information (ESI) available. See DOI: 10.1039/c6ra27736e

magnetic mesoporous silica microspheres exhibit attractive physical and chemical properties as a sorbent, particularly due to their large surface area and associated advantages in diffusion rates, low toxicity, chemically modifiable surface and ease of separation under external magnetic fields.[25,26] Additionally, they can withstand fast flow chromatographic separations, unlike the traditional supports for IMAC based on soft-gel matrices such as cross-linked agarose and dextran. Until recently, the synthesis of monodisperse porous silica microspheres in the 3–10 μm range were still considered to be difficult.[27] More recent sorbent synthesis studies were aimed at decreasing the sorbent size distribution, increasing pore volumes and magnetic nanoparticle loadings or simplifying the synthesis process.[25,26,28–30] In our recent studies, a new synthesis protocol was developed for the magnetic SiO_2 microspheres (Mag-SiO_2) in the monodisperse and porous form. The sorbent synthesized from Mag-SiO_2 microspheres was effectively used for highly selective enrichment of phosphopeptides from human serum *via* immobilized Ti(IV) affinity chromatography.[31] In this study, (i) a magnetic IMAC sorbent functionalized with Ni^{2+} was designed in the form of monodisperse-porous silica microspheres with bimodal pore-size distribution; (ii) the IMAC sorbent exhibited a superior and more stable magnetic behaviour with respect to the currently produced sorbents in the form of magnetic core/shell nanoparticles; (iii) the saturation magnetization of the sorbent allowed the faster isolation of target His-tagged protein from cell-lysate with the isolation periods shorter than 10 s; (iv) the isolation of target His-tagged protein with a purity higher than 95% was achieved which was a considerably higher value with respect to the recently reported similar sorbents.

2. Experimental

2.1 Materials

Glycidyl methacrylate (GMA), methacrylic acid (MAA), and ethylene dimethacrylate (EDMA) were supplied from Aldrich Chem. Co. (Milwaukee, WI, USA) and used in the synthesis of monodisperse-porous poly(methacrylic acid-*co*-ethylene dimethacrylate), poly(MAA-*co*-EDMA) microspheres, without further purification. Ethylbenzene (EB), tetrahydrofuran (THF), absolute ethanol (EtOH) were of HPLC grade and supplied from Aldrich. Sodium lauryl sulfate (SLS), $FeCl_3 \cdot 6H_2O$, and $FeCl_2 \cdot 4H_2O$, and $NiCl_2$ were obtained from Sigma Chemical Co. (St. Louis, MO, USA). 2,2′-Azobisisobutyronitrile (AIBN), was supplied from Merck A.G. (Darmstadt, Germany) and recrystallized from methanol before use. Benzoyl peroxide (BPO), tetrabutylammonium iodide (TBAI), tetraethyl orthosilicate (TEOS), 2-propanol (IPA), ammonium hydroxide (NH_4OH), iminodiacetic acid (IDA), (3-glycidyloxypropyl)trimethoxysilane (GLYMO), and sodium hydroxide (NaOH) were purchased from Sigma.

For protein expression, preparation of cell lysate, and SDS-PAGE analysis of purified proteins: Luria–Bertani (LB) medium was supplied from Merck, Germany. *E. coli* BL21 Star (DE3) strain was purchased from Thermo Fisher Scientific (Waltham, MA, USA). pET28a-GFP-6xHis plasmid was kindly

provided by Prof. Dr Matthew P. DeLisa. Isopropyl β-D-1-thiogalactopyranoside (IPTG), sodium chloride (NaCl), kanamycin sulfate, imidazole, D-glucose monohydrate, acrylamide/bisacrylamide 30% w/w solution, sodium dodecyl sulfate (SDS), ammonium persulfate, tetramethylethylenediamine (TEMED), bovine serum albumin (BSA) and Bradford reagent were obtained from Sigma. Protein ladder (Precision Plus Protein Dual Color standard) and Bio-Safe™ Coomassie stain were from Bio-Rad, USA. Deionized (DI) water (18.2 MΩ cm) was used in all runs (Direct-Q®3 UV System, Millipore S.A.S, Molsheim, France).

2.2 Synthesis of magnetic SiO_2 (SiO_2@Mag-SiO_2) microspheres

The poly(glycidyl methacrylate), poly(GMA), seed latex 2.1 μm in size was synthesized by dispersion polymerization of GMA.[32] Monodisperse-porous poly(methacrylic acid-*co*-ethylene dimethacrylate), poly(MAA-*co*-EDMA) microspheres 6 μm in size were obtained by using multi-step microsuspension polymerization technique.[33,34] The magnetization of poly(MAA-*co*-EDMA) microspheres was performed as described elsewhere.[35] The magnetic poly(MAA-*co*-EDMA) microspheres were used as a template for synthesis of monodisperse, magnetic SiO_2 microspheres. Briefly, the poly(MAA-*co*-EDMA) microspheres were dispersed in an aqueous solution containing TBAI, ammonia, 2-propanol and distilled water for 1 hour under mechanical stirring. TEOS solution (in IPA containing 50 w/w%) was added dropwise into the solution and stirred for 24 h at R.T. The formed silica-gel/poly(MAA-*co*-EDMA) composite microspheres were then separated by a magnet and washed with IPA and distilled water 3 times. The magnetic microspheres were dried in vacuum at 60 °C for 24 h. The calcination was carried out at 450 °C for 10 h for formation of the magnetic, monodisperse SiO_2 microspheres. Finally, SiO_2 coating onto the Mag-SiO_2 microspheres (SiO_2@Mag-SiO_2) was done with the same process as described above.[31]

2.3 Synthesis of iminodiacetic acid attached magnetic SiO_2 (IDA–GLYMO@SiO_2@Mag-SiO_2) microspheres

The synthesis of iminodiacetic acid–(3-glycidoxypropyl)trimethoxysilane (IDA–GLYMO) precursor was performed by using a modified form of the protocol reported previously:[36] IDA (0.53 g) was dissolved in 10 mL of DDI water, and pH of solution was adjusted to 11.0 with 10.0 M NaOH. The obtained solution was transferred into a Pyrex® reactor placed in an ice-bath at 0 °C, and 0.4 mL of GLYMO was slowly added under stirring. The solution was heated to 65 °C for 6 h with stirring, subsequently placed into an ice-bath for 10 min to decrease the temperature to 0 °C. 0.4 mL of GLYMO was again added and the temperature was increased to 65 °C for another 6 h under stirring. Finally, pH of IDA–GLYMO solution was adjusted to 3 with concentrated HCl. In order to attach IDA–GLYMO precursor onto the SiO_2@Mag-SiO_2 microspheres, 0.2 g of microspheres were added to IDA–GLYMO solution at pH 3 and the resulting dispersion was heated at 95 °C for 2 h with mechanical stirring. The resulting IDA–GLYMO@SiO_2@Mag-SiO_2 microspheres

were extensively washed with DDI water and finally dispersed in DDI water.

2.4 Ni²⁺ attachment onto IDA–GLYMO@SiO₂-Mag-SiO₂ microspheres

Ni²⁺-immobilized IDA–GLYMO@SiO₂@Mag-SiO₂ (Ni²⁺–IDA–GLYMO@SiO₂@Mag-SiO₂) microspheres were prepared by the incubation of IDA–GLYMO@SiO₂@Mag-SiO₂ microspheres (20 mg) in 0.25 M aqueous NiCl₂ solution at RT for 2 h under gentle stirring. The obtained Ni²⁺–IDA–GLYMO@SiO₂@Mag-SiO₂ microspheres were collected by magnetic separation and washed with distilled water several times to remove free Ni²⁺ ions. In this case, each Ni²⁺ ion coordinates to more than one carboxyl groups (–COOH) *via* metal(II) carboxyl chemistry.

2.5 Characterization of magnetic microspheres

The average size and size distribution of magnetic microspheres were determined by a scanning electron microscope (FEI, Quanta 200 FEG, U.S.A.). The specific surface area was determined by a surface area and pore size analyzer (Quantachrome, Nova 2200E, U.K.) using nitrogen adsorption–desorption method. X-ray diffraction (XRD) spectra of microspheres were obtained using a Rigaku X-ray diffractometer (Ultima IV, Japan). To investigate the formation of SiO₂ coating on Mag-SiO₂ microspheres, X-ray photoelectron spectroscopy (XPS, Thermo-K-Alpha-Monochromated high-performance XPS Spectrometer) with an Al K-Alpha source gun was performed at 1.4 kV focus voltage, 6 mA beam current, and 400 μm of spot size. The magnetization curves of Mag-SiO₂, SiO₂@Mag-SiO₂, and IDA–GLYMO–SiO₂@Mag-SiO₂ microspheres were obtained by a vibrating sample magnetometer (Cryogenic Limited, PPM system, UK). All of the measurements were carried out at room temperature (*i.e.* 300 K) and the saturation magnetization (M_s; emu g⁻¹) values were obtained from hysteresis loops. The carboxyl content of IDA–GLYMO@SiO₂@Mag-SiO₂ microspheres was determined by potentiometric titration (mmol IDA per g microspheres).

2.6 Protein expression and preparation of cell-free extracts

In this study, green fluorescent protein (GFP) was selected as the model His-tagged recombinant protein and used in most of the protein isolation runs by IMAC. His-tagged endoglucanase (Cel5A)[37] was used as a second target protein purified from *E. coli* lysate. Recombinant protein production was carried out in batch cultures using 250 mL air-filtered shake flasks containing 30 mL Luria–Bertani (LB) medium, composed of 10 g L⁻¹ peptone, 5 g L⁻¹ yeast extract, 10 g L⁻¹ NaCl and supplemented with 50 μg mL⁻¹ kanamycin. Overnight cultures of *E. coli* BL21 Star (DE3), transformed with pET28a-GFP-6xHis plasmid or pTrc-Cel5A-6xHis plasmid, were incubated at 37 °C until the optical density at 600 nm (OD600) reached 0.45 and then induced with 200 μM IPTG for 24 h at 30 °C, 150 rpm. Cell growth was followed using UV-Vis spectrophotometer (GEN-ESYS 10S, Thermo Scientific). At the end of the recombinant protein production phase, cells were harvested by centrifugation at 8000 g for 10 min at 4 °C and stored at −20 °C until use.

Prior to protein purification, protein stock solution from the cell lysate was obtained by sonication of cells (2 cycles of 30 s sonication, 1 min on ice) followed by centrifugation at 13 000 g for 10 min at 4 °C.

2.7 His-tagged recombinant protein binding and separation *via* magnetic composite microspheres

Ni²⁺–IDA–GLYMO@SiO₂@Mag-SiO₂ microspheres (1, 5, 10, 20, 50 mg) were suspended in 1 mL of binding buffer (20 mM phosphate buffer, 1 M NaCl, pH 7.0) by vortexing. The magnetic microspheres were washed with binding buffer three times, followed by magnetic separation. In a typical isolation process performed with *E. coli* lysate, the protein stock solution (0.4 mL) was added onto the Ni²⁺–IDA–GLYMO@SiO₂@Mag-SiO₂ microspheres incubated at room temperature for 30 min with shaking. His-tagged protein-loaded Ni²⁺–IDA–GLYMO@SiO₂@Mag-SiO₂ microspheres were collected by a magnet and washed with 0.4 mL of binding buffer two times to remove the non-specifically adsorbed proteins. Subsequently, the trapped His-tagged or Histidine-rich proteins were directly eluted from the microspheres with imidazole (0.2 mL, 500 mM) five times. The eluted proteins in each step (including the stock, supernatant and eluate solutions) were collected and stored at 4 °C until further analyses. The reusability of Ni²⁺–IDA–GLYMO@SiO₂@Mag-SiO₂ microspheres was investigated by performing five successive His-tagged GFP isolations under the same conditions. The sorbent was washed with 20 mM MES buffer (pH 5.0) containing 100 mM NaCl, DDI water and the adsorption buffer between successive purifications.

Protein concentration in an eluate solution was determined in triplicates using Bradford reagent (Sigma) according to manufacturer's instructions, using bovine serum albumin (BSA) as standard. Purified proteins were analyzed by sodium dodecyl sulfate polyacrylamide gel electrophoresis (SDS-PAGE) including a protein ladder. Separated proteins were stained with coomassie stain and visualized by GelDoc EZ imaging system (Bio-Rad). The Image Lab 5.1 software (Bio-Rad) was used to calculate the protein purification parameters (desorption yield, isolation yield and purity), based on total protein concentration and analysis of the PAGE image. The desorption yield for the target protein, GFP was defined as the weight ratio of GFP eluted from the sorbent to GFP adsorbed onto the sorbent. The isolation yield of GFP was defined as the weight ratio of GFP eluted from the sorbent to GFP loaded to the sorbent. The purity of target protein in the eluate was given as the weight ratio of GFP to the total protein.

3. Results and discussion

3.1 Synthesis and characterization of magnetic sorbent

The loss of saturation magnetization by increasing the number of functional shells around the magnetic core is an important drawback of the currently available magnetic core/shell nanoparticles used as sorbent in IMAC applications.[12,21,38] In the present study, a magnetic IMAC sorbent with stable magnetic behaviour and sufficiently high saturation magnetization was developed for selective isolation of His-tagged proteins. The

monodisperse-porous poly(MAA-*co*-EDMA) microspheres 6 μm in size were produced by a modified seeded polymerization protocol.[33,34] The magnetization of poly(MAA-*co*-EDMA) microspheres was carried out by the precipitation of magnetic Fe_3O_4 nanoparticles into the porous interior of microspheres.[35] The magnetic polymer microspheres were then utilized as a template for the synthesis of monodisperse silica microspheres. The presence of NH^{4+} cations in the reaction medium led to the hydrolysis and condensation reaction of TEOS onto the magnetic polymer microspheres. After calcination of composite polymer/silica gel microspheres at 450 °C, magnetic monodisperse SiO_2 microspheres (Mag-SiO_2) were synthesized 6.0 μm in size. Finally, a thin layer of SiO_2 was coated onto the Mag-SiO_2 microspheres to prevent the leaching of immobilized magnetic nanoparticles during the attachment of IDA–GLYMO silane precursor onto the microspheres.[31,36]

IDA–GLYMO silane precursor was synthesized by the conjugation of imine groups of IDA to the epoxy groups of GLYMO silane (Fig. 1A). Then, IDA–GLYMO silane was covalently attached onto SiO_2@Mag-SiO_2 microspheres by the reaction between hydroxyl groups of microspheres and trimethoxysilane groups of GLYMO. The metal-chelate formation on the SiO_2@Mag-SiO_2 microspheres was achieved by the interaction of Ni^{2+} ions with the carboxyl groups of IDA (Fig. 1B).

The SEM photographs of porous Mag-SiO_2, SiO_2@Mag-SiO_2, and IDA–GLYMO@ SiO_2@Mag-SiO_2 microspheres are given in Fig. 2A–C, respectively. All of the microspheres were obtained with narrow size distribution and porous surface morphology. According to SEM photos, no significant change was observed both in the mean size and the surface morphology of Mag-SiO_2 microspheres by coating with SiO_2 layer and attachment of IDA–GLYMO silane precursor (Fig. 2B and C).

The mean size values of microspheres, the coefficient of variation values (CV%) calculated from SEM photos showing the size distribution and the specific surface area (SSA) values, are given in Table 1. The pore-size distributions of Mag-SiO_2 and SiO_2@Mag-SiO_2 microspheres determined by nitrogen adsorption desorption method is given in Fig. 3A and B, respectively. This figure clearly showed the bimodal character of pore size distribution of SiO_2@Mag-SiO_2 microspheres including both mesopores and macropores, lying between 6–50
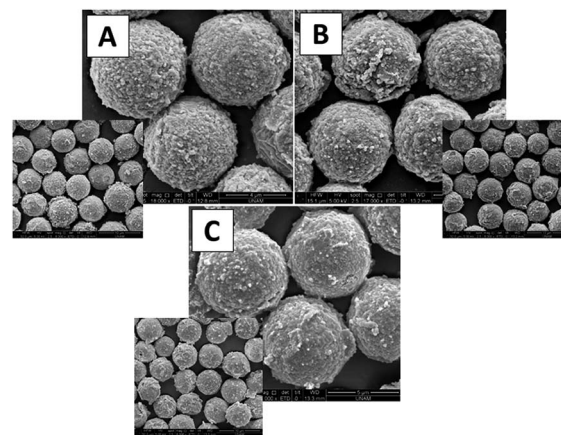

Fig. 2 SEM images of (A) Mag-SiO_2, (B) SiO_2@Mag-SiO_2, and (C) IDA–GLYMO@SiO_2@Mag-SiO_2 microspheres.

and 50–140 nm, respectively. Note that Ti(IV) attached and polydopamine coated form of SiO_2@Mag-SiO_2 microspheres was used as sorbent for phosphopeptide enrichment from human serum *via* immobilized metal affinity chromatography.[31] In the referred study, SSA of Mag-SiO_2 microspheres was determined as 250 $m^2 g^{-1}$.[31] SSA of SiO_2@Mag-SiO_2 was markedly lower with respect to Mag-SiO_2 microspheres (Table 1). The comparison of Fig. 3A and B showed that the sharp peak obtained for mesopore fraction at 3.5 nm in the pore size distribution of Mag-SiO_2 microspheres disappeared by the formation of SiO_2 coating. Then, the marked decrease in SSA (*i.e.* from 245 to 45 $m^2 g^{-1}$) should be explained by filling of mesopores of Mag-SiO_2 microspheres with the SiO_2 layer formed. The pore size distribution measurements also showed that no significant change occurred in the mean pore size by the formation of SiO_2 shell and IDA–GLYMO attachment performed in the acidic medium (pH: 3) [Table 1].

X-ray diffraction spectra of poly(MAA-*co*-EDMA) microspheres, magnetic poly(MAA-*co*-EDMA) microspheres utilized as template for the production of Mag-SiO_2 microspheres, Mag-SiO_2 microspheres and SiO_2@Mag-SiO_2 microspheres are given in Fig. 3. XRD spectrum of poly(MAA-*co*-EDMA) microspheres showed their amorphous character (Fig. 3C). The peaks belonging to the crystalline Fe and Si phases in magnetic poly(MAA-*co*-EDMA), Mag-SiO_2 and SiO_2@Mag-SiO_2 microspheres were clearly observed in the related spectra (Fig. 3D).
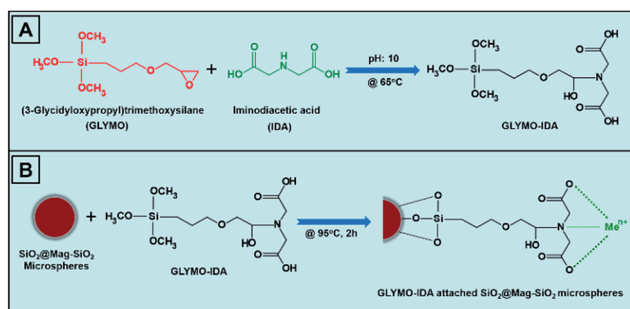

Fig. 1 (A) The synthetic route for preparation of IDA–GLYMO silane precursor and (B) immobilization of IDA–GLYMO onto SiO_2@Mag-SiO_2 microspheres and Ni^{2+} immobilization on the IDA–GLYMO@SiO_2@Mag-SiO_2 microspheres.

Table 1 The morphological properties of magnetic silica microspheres functionalized with different shell layers[31]

Microsphere type	Mean size (μm)	CV (%)	SSA^a ($m^2 g^{-1}$)	Mean pore size (nm)
MagSiO$_2$^{b}	6.4	4.3	245	2.02
SiO_2@MagSiO$_2$	6.6	4.1	45	1.95
IDA–GLYMO@SiO_2@MagSiO$_2$	6.6	4.2	16	2.02

^{a} SSA was determined according to BET model. ^{b} Mean size and CV values.[31]
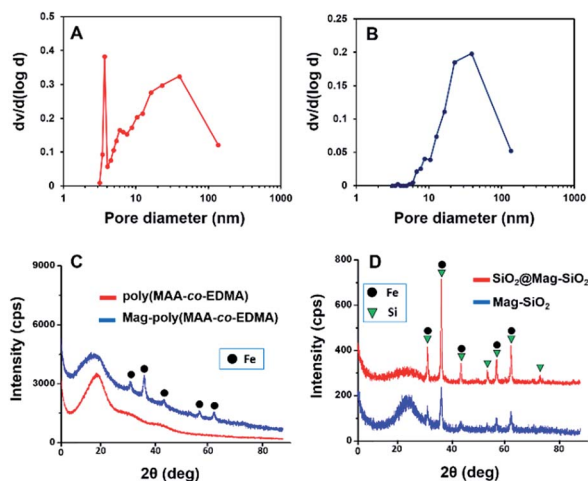
Fig. 3 Pore-size distribution of (A) Mag-SiO$_2$ and (B) SiO$_2$@Mag-SiO$_2$ microspheres determined by nitrogen adsorption desorption method; X-ray diffraction spectra of (C) poly(MAA-*co*-EDMA) microspheres, (D) magnetic poly(MAA-*co*-EDMA) microspheres, (E) Mag-SiO$_2$ microspheres, and (F) SiO$_2$@Mag-SiO$_2$ microspheres. In (A) and (B), *v* is the pore volume and *d* is the pore diameter.

XPS was used to investigate the formation of SiO$_2$ coating on the Mag-SiO$_2$ microspheres by scanning a surface area with a diameter of 400 μm. XPS spectra of Mag-SiO$_2$ and SiO$_2$@Mag-SiO$_2$ microspheres are given in Fig. 4. Si 2p bands obtained for Mag-SiO$_2$ and SiO$_2$@Mag-SiO$_2$ microspheres are compared in Fig. 4B. As seen here, Si 2p band shifted from 104.28 to 103.78 eV by the formation of SiO$_2$ layer on the surface of Mag-SiO$_2$ microspheres. A similar comparison was also made for O 1s bands obtained for Mag-SiO$_2$ and SiO$_2$@Mag-SiO$_2$ microspheres in Fig. 4C. As also seen here, a similar shift from 533.48 to 532.98 eV was observed for O 1s band. These shifts can be evaluated as clear evidences showing the formation of SiO$_2$ layer on Mag-SiO$_2$ microspheres as described in the literature.[39,40] On the other hand, a mass increase of 45.0% w/w obtained by

coating of Mag-SiO$_2$ microspheres can be also evaluated as a gravimetric finding showing the deposition of SiO$_2$ onto the Mag-SiO$_2$ microspheres.

The magnetization behaviour of Mag-SiO$_2$ and SiO$_2$@Mag-SiO$_2$ microspheres were investigated in our previous study.[31] The results showed that all microspheres exhibited super-paramagnetic behaviour and the highest saturation magnetization value was obtained with Mag-SiO$_2$ microspheres ($M_s = 26.0$ emu g^{-1}). The saturation magnetization values of SiO$_2$@-Mag-SiO$_2$, and IDA–GLYMO@SiO$_2$@Mag-SiO$_2$ microspheres were determined as 23.5 and 22.1 emu g^{-1}, respectively (Fig. 4D).[31] The slight decrease observed in the saturation magnetization was explained by the mass increase due to the formation of SiO$_2$ shell on Mag-SiO$_2$ microspheres. The minimum saturation magnetization for performing an effective separation by a magnetic sorbent was reported as 16.3 emu g^{-1}.[38] Hence, the commonly accepted criterion was satisfied by IDA–GLYMO@SiO$_2$@Mag-SiO$_2$ microspheres. Moreover, the use of a large particles like 6 μm in size facilitates the separation of magnetic sorbent from the liquid medium under external magnetic field during the isolation of His-tagged protein. The sorbent with the saturation magnetization of 22.1 emu g^{-1} could be completely isolated from the liquid medium by means of an external magnet within less than 5 seconds under the conditions used for the isolation of His-tagged GFP in this study.

In the literature, a marked decrease in the saturation magnetization was mostly observed by the formation of additional shell layers around the magnetic nanoparticles.[12,21,41] In the case of Ni^{2+} attached and poly(*n*-vinylimidazole) coated magnetic Fe$_3$O$_4$ microspheres used for the separation of His-tagged proteins, approximately 3-fold decrease in the saturation magnetization of magnetic core (*i.e.* 67.2 emu g^{-1}) was observed by the formation of poly(*n*-vinylimidazole) core and Ni^{2+} attachment (*i.e.* 19.5 emu g^{-1}).[12] A similar remarkable decrease (5-fold) in the saturation magnetization of magnetic Fe$_3$O$_4$ core was also observed by the synthesis of Fe$_3$O$_4$@NiSiO$_3$ nanoparticles with yolk–shell structure used for the magnetic isolation of His-tagged proteins.[21] In another study, the saturation magnetization values were measured as 42.2 and 8.8 emu g^{-1} for Fe$_3$O$_4$ and Fe$_3$O$_4$@NiSiO$_3$ nanostructures, respectively. Ma *et al.* also synthesized a sorbent for the enrichment of phosphopeptides by starting from a magnetic colloid nanocrystal cluster core with the saturation magnetization of 67.5 emu g^{-1}.[41] The saturation magnetization of the final composite sorbent containing polymethacrylic acid and polyethyleneglycol-monophosphate shell layers around the magnetic core was determined as 8.3 emu g^{-1} with almost an 8 fold-decrease with respect to the starting material. In this study, only a small change in the saturation magnetization from 26.0 to 22.1 emu g^{-1}, corresponding to a decrease lower than 15% was observed by the formation of SiO$_2$ shell coating and the attachment of IDA–GLYMO silane precursor onto the microspheres. Based on this finding, one can conclude that, "a new magnetic IMAC sorbent carrying Ni^{2+} cations suitable for His-tagged protein isolation" was obtained in the form of "monodisperse-porous SiO$_2$ microspheres" with "sufficiently high saturation magnetization and stable magnetic behavior" "with respect to "composite
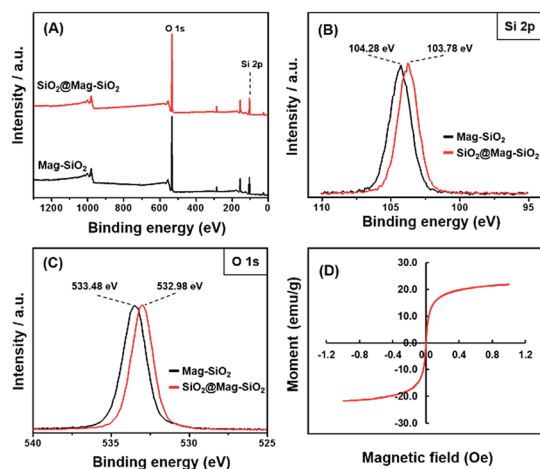

Fig. 4 XPS spectra of Mag-SiO$_2$ and SiO$_2$@Mag-SiO$_2$ microspheres, (A) full scan, (B) Si 2p, (C) O 1s, (D) magnetization curve of mono-disperse-porous IDA–GLYMO@SiO$_2$@Mag-SiO$_2$ microsphere.

magnetic nanoparticles" commonly proposed for the specific isolation/purification of His-tagged proteins.

3.2 Ni²⁺–IDA–GLYMO@SiO₂@Mag-SiO₂ microspheres as sorbent for purification of His-tagged target protein

To test the performance of Ni²⁺–IDA–GLYMO@SiO₂@Mag-SiO₂ microspheres for the purification of His-tagged target protein *via* IMAC, we induced the expression of His-tagged-GFP in an *E. coli* culture, isolated His-tagged GFP by an IMAC protocol involving the adsorption of GFP onto the sorbent and the elution of adsorbed GFP from the sorbent by imidazole buffer, then analyzed the eluted proteins *via* SDS-PAGE gel electrophoresis (Fig. 5).

After purification with Ni²⁺–IDA–GLYMO@SiO₂@Mag-SiO₂ microspheres, the His-tagged GFP was clearly distinguishable in the elution lane, with negligible amounts in the wash lanes (W1 and W2), indicating successful purification of the target protein in the complex *E. coli* lysate (Fig. 6).

SDS-PAGE analysis of purified His-tagged protein from *E. coli* lysate by using different amounts of sorbent is given in Fig. 7. As seen here, His-tagged GFP was effectively purified by Ni²⁺–IDA–GLYMO@SiO₂@Mag-SiO₂ microspheres from *E. coli* lysate, even by using minimal amount of sorbent (1 mg) under equilibrium conditions. The nonspecific adsorption of contaminating proteins decreased significantly by decreasing the sorbent amount. While the target protein was obtained with >95% purity in E1 with 1 mg of sorbent, the same purity was obtained in E2 with 5–10 mg of sorbent and in E3 with 20 mg of sorbent (Fig. 7). Naturally, to obtain the purity as high as that observed in E1 with 1 mg of sorbent, the number of elutions should be increased with increasing amount of sorbent. On the other hand, the amount of target protein isolated with high purity also decreased by decreasing the amount of sorbent, as expected.

The effect of sorbent concentration on the His-tagged GFP adsorption (Q: mg GFP per g sorbent) under equilibrium conditions is shown in Fig. 8A. It is clear that the equilibrium adsorption of His-tagged GFP decreased with the increasing amount of sorbent. The highest His-tagged GFP adsorption was observed as 87.4 mg GFP per g sorbent with the lowest sorbent amount (*i.e.* 1 mg). The equilibrium His-tagged GFP adsorption
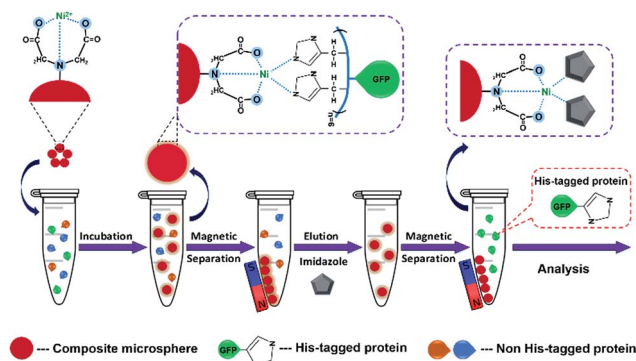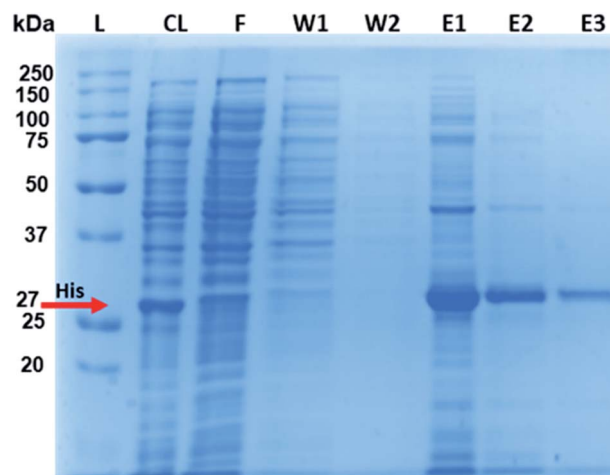

Fig. 6 SDS-PAGE analysis of affinity purification steps of the His-tagged protein from *E. coli* cell lysate (CL), flowthrough (F), wash 1 (W1), wash 2 (W2), elutions 1–3 (E1–E3), using 20 mg of sorbent in 0.4 mL of adsorption medium at pH 7.0.

decreased from 87.4 to 3.4 mg GFP per g sorbent by increasing the sorbent amount from 1 to 50 mg and a lower plateau was observed with the sorbent amounts higher than 10 mg in the batch studied (Fig. 8A). The effects of sorbent amount on both desorption yield and isolation yield of His-tagged GFP is given in Fig. 8B. As expected, the isolation yield increased with the increasing amount of sorbent. The maximum isolation yield was obtained as 68.0% w/w with the highest sorbent amount (*i.e.* 50 mg). Interestingly, an increase in desorption yield was also observed with the increasing sorbent amount. The low desorption yields obtained with the lower amounts of sorbent can be ascribed to the formation of increasing irreversible, nonspecific interactions between GFP and sorbent when the GFP/sorbent weight ratio was increased.
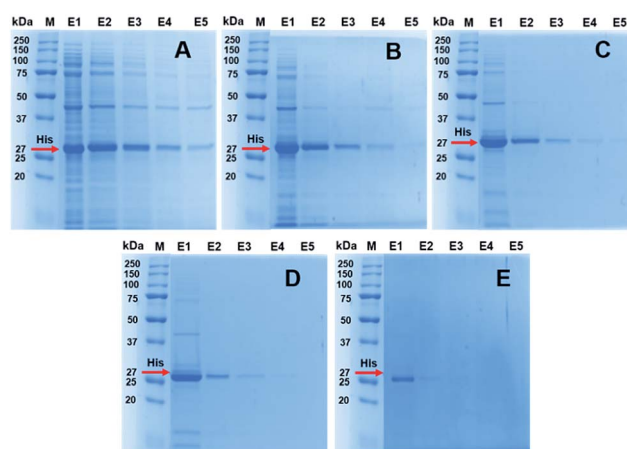

Fig. 7 SDS-PAGE analysis of the purified His-tagged protein from *E. coli* lysate by using different amount of sorbent: (A) 50 mg, (B) 20 mg, (C) 10 mg, (D) 5 mg, and (E) 1 mg. Adsorption medium: 0.4 mL. Lane M: the protein molecular weight marker, Lane E1–E5: after purification with Ni²⁺–IDA–GLYMO@SiO₂@Mag-SiO₂ microspheres and eluted with imidazole. The arrow points to target protein, His-tagged GFP.

Fig. 5 The schematic representation of His-tagged protein purification by using Ni²⁺–IDA–GLYMO@SiO₂@Mag-SiO₂ microspheres.
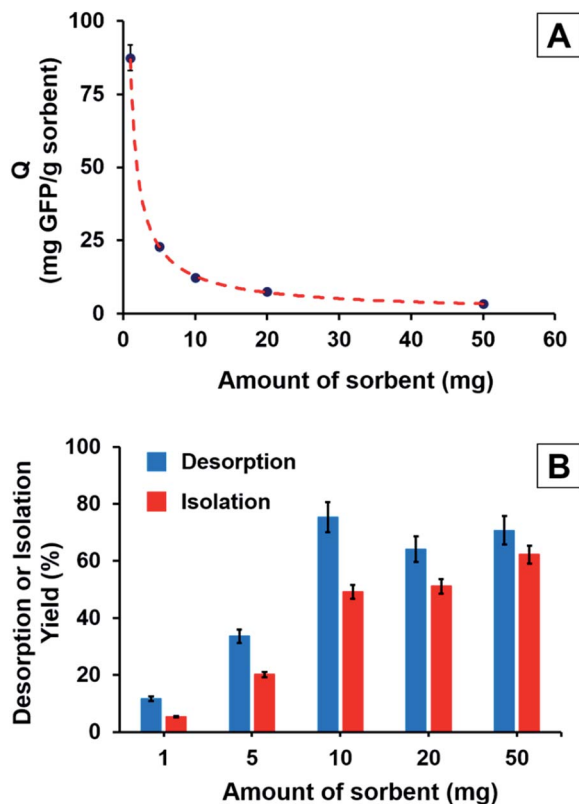
Fig. 8 (A) The effect of sorbent concentration on equilibrium His-tagged GFP adsorption, (B) the variation of His-tagged GFP desorption yield and isolation yield with the sorbent concentration. Adsorption medium: 0.4 mL. Desorption medium: 0.2 mL.

The effect of desorption buffer concentration on both the isolation and desorption yields of His-tagged GFP is given in Fig. 9. Here, 10 mg of sorbent was incubated with 0.4 mL of *E. coli* lysate with the initial GFP concentration of 0.5 mg mL^{-1} for 30 min at room temperature. Both isolation yield and desorption yield increased with increasing concentration of imidazole. The highest desorption and isolation yields were obtained as 94% and 68 w/w, respectively, using the imidazole concentration of 0.5 M. However, the imidazole concentration of
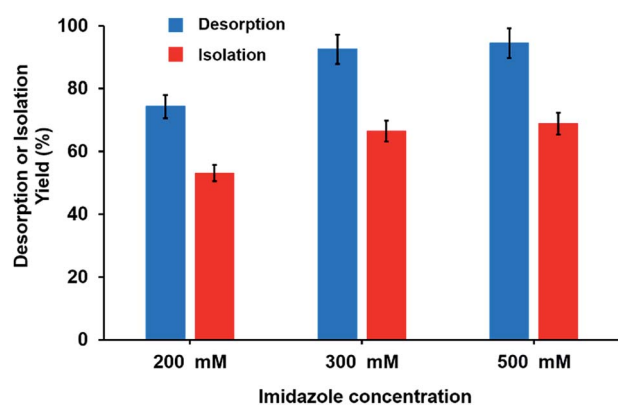

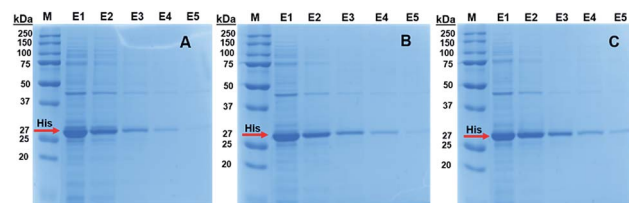Fig. 9 The effect of imidazole concentration on the isolation and desorption yield of purified His-tagged GFP.

Fig. 10 SDS-PAGE analysis of purified His-tagged protein from *E. coli* lysate by using different imidazole concentrations: (A) 0.5 M, (B) 0.3 M, (C) 0.2 M. Lane M: the protein molecular weight marker, lane E1–E5: after purification with Ni^{2+}–IDA–GLYMO@SiO$_2$@Mag-SiO$_2$ microspheres and eluted with imidazole. The arrow points to target protein, His-tagged GFP.

0.2 M was sufficient to obtain a satisfactory isolation yield (*i.e.* 54% w/w) from Ni^{2+}–IDA–GLYMO@SiO$_2$@Mag-SiO$_2$ microspheres.

SDS-PAGE analysis of purified His-tagged protein from *E. coli* lysate by using different imidazole concentrations is given in Fig. 10. As seen here, while the purification of His tagged-GFP was generally achieved with high purity for all imidazole concentrations studied, purity of target protein in the eluates increased with decreasing imidazole concentration. Moreover, two commercial resins were also studied side-by-side with Ni^{2+}–IDA–GLYMO@SiO$_2$@Mag-SiO$_2$ microspheres for His-tagged protein (*i.e.* GFP) isolation from *E. coli* lysate. The purity of isolated GFP in the eluates was almost the same for all sorbents tried (Fig. S1†).

The comparison of His-tagged protein purification performance of the sorbent proposed in this study with those developed previously by different researches is given in Table 2. As seen here, Ni^{2+}–IDA–GLYMO@SiO$_2$@Mag-SiO$_2$ microspheres had a medium level of equilibrium adsorption capacity among the sorbents developed for His-tagged protein purification by IMAC. On the other hand, the purity of isolated His-tag protein was lower than 95% for most of the sorbents listed in Table 2. Only two sorbents, Fe$_3$O$_4$/Au–ANTA–Co^{2+} nanoparticles and MnFe$_2$O$_4$@SiO$_2$@NH$_2$@2AB–Ni nanoparticles allowed the isolation of His-tagged proteins with the purity higher than 95%. As mentioned above, GFP could be also isolated with the purity higher than 95%, using the Ni^{2+}–IDA–GLYMO@SiO$_2$@Mag-SiO$_2$ microspheres. Hence, the purity of His-tagged protein isolated with the proposed sorbent was higher with respect to most of the previously developed IMAC sorbents (Table 2).

The reusability of Ni^{2+}–IDA–GLYMO@SiO$_2$@Mag-SiO$_2$ microspheres was investigated by performing five successive His-tagged GFP isolations under the same conditions. The variation of equilibrium His-tagged GFP adsorption with the cycle number is given in Fig. 11.

As seen here, a decrease of 17% was observed in the equilibrium His-tagged GFP adsorption at the end of fifth cycle. Fig. 11 showed that Ni^{2+}–IDA–GLYMO@SiO$_2$@Mag-SiO$_2$ microspheres had a satisfactory reusability behaviour similar to the IMAC sorbents previously used for His-tagged protein purifications.[21,22]

The isolation performance of Ni^{2+}–IDA–GLYMO@SiO$_2$@-Mag-SiO$_2$ was also determined using His-tagged endoglucanase

Table 2 Properties of different adsorbents for purification of His-tagged proteins[a]

Affinity support	Sample	Purity of His-tagged protein (%)	Adsorption capacity (mg protein per g sorbent)	Ref.
Fe$_3$O$_4$@SiO$_2$@NiAl-LDH microspheres	His-tagged protein from cell lysate	N/A	239	15
Fe$_3$O$_4$/Au–ANTA–Co^{2+} nanoparticles	E. coli cell lysate	96	74	7
CuFe$_2$O$_4$ magnetic nanocrystal clusters	His-rich protein (bovine haemoglobin)	<95[b]	4475	20
Yolk–shell Fe$_3$O$_4$@NiSiO$_3$ nanostructures	E. coli cell lysate	91	220	21
Ni^{2+}–zeolite/ferrosphere and Ni^{2+}–silica/ferrosphere beads	E. coli cell lysate	95	1.5–3.0	28
MnFe$_2$O$_4$@SiO$_2$@NH$_2$@2AB–Ni nanoparticles	E. coli cell lysate	>95[b]	220	42
NiCoMnO$_4$ particles	E. coli cell lysate	60	43	43
Fe$_3$O$_4$/PMG/IDA–Ni^{2+} nanoparticles	E. coli cell lysate	<90[b]	103	22
Fe$_3$O$_4$/PVIM–Ni^{2+} microspheres	E. coli cell lysate	<90[b]	248	12
SiO$_2$@IDA/MAPS–Ni^{2+} nanoparticles	E. coli cell lysate	52.9	3.6	24
Ni^{2+}–IDA–GLYMO@SiO$_2$@Mag-SiO$_2$	E. coli cell lysate	>95	87	This work

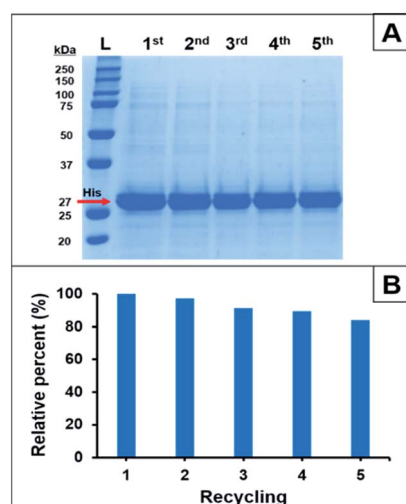[a] N/A: not available. [b] Determined by image analysis of the SDS-PAGE figures provided.

Fig. 11 (A) SDS-PAGE analysis of purified His-tagged protein by Ni^{2+}–IDA–GLYMO@SiO$_2$@Mag-SiO$_2$ microspheres reused up to five times (lanes 2–6); (B) change of equilibrium His-tagged GFP adsorption for Ni^{2+}–IDA–GLYMO@SiO$_2$@Mag-SiO$_2$ microspheres, given relative to equilibrium adsorption (mg GFP per g sorbent) obtained in the first use.

(Cel5A) as a second target protein purified from E. coli lysate. For Cel5A, the desorption yield, the isolation yield and the purity in the second eluate were determined as 92%, 38% and ≥95%, respectively (Fig. S2†). These values were similar to those obtained for His-tagged GFP.

4. Conclusions

A new magnetic sorbent based on monodisperse-porous silica microspheres 6 μm in size was proposed for His-tagged protein purification by IMAC. The sorbent exhibited a stable and superior magnetic behaviour with respect to the commonly available composite sorbents in the form of magnetic core–shell nanoparticles carrying functional shells.

The base material, monodisperse-porous silica microspheres with bimodal pore-size distribution were synthesized by a developed staged-shape templated hydrolysis & condensation protocol. The silica microspheres were then converted into an IMAC sorbent via functionalization with Ni^{2+} via silane chemistry. The purification of His tagged-GFP obtained from E. coli lysate, as a model protein was investigated in batch-fashion. GFP isolation yields up to 68% w/w with the purity of higher than 95% were achieved using the proposed sorbent.

The satisfactory isolation performance of the sorbent was ascribed to bimodal porous structure of the base-material. The developed sorbent has further potential as follows: (i) the base material (i.e. magnetic monodisperse-porous silica microspheres) can be also used as starting material for the synthesis of various sorbents and stationary phases for different modes of affinity chromatography, (ii) the size, porous properties and magnetic properties of the sorbent are also suitable for continuous affinity chromatography applications particularly in the microfluidic systems, (iii) the size and porous properties of non-magnetic form of the sorbent are also suitable for obtaining various packed-columns both in conventional and micro-liquid chromatography applications, (iv) the magnetic sorbent can be also applied to the purification of other His-tagged proteins from various biological sources.

References

1 L. Doyle, J. Hallinan, J. Bolduc, F. Parmeggiani, D. Baker, B. L. Stoddard and P. Bradley, *Nature*, 2015, **528**, 585–588.

2 H. M. Hsu, C. H. Chu, Y. T. Wang, Y. Lee, S. Y. Wei, H. W. Liu, S. J. Ong, C. P. Chen and J. H. Tai, *J. Biol. Chem.*, 2014, **289**, 19120–19136.

3 C. A. Brimacombe, H. Ding and J. T. Beatty, *Mol. Microbiol.*, 2014, **92**, 1260–1278.

4 D. W. Wood, *Curr. Opin. Struct. Biol.*, 2014, **26**, 54–61.

5 S. Lata, A. Reichel, R. Brock, R. Tampe and J. Piehler, *J. Am. Chem. Soc.*, 2005, **127**, 10205–10215.

6 I. S. Lee, N. Lee, J. Park, B. H. Kim, Y. W. Yi, T. Kim, T. K. Kim, I. H. Lee, S. R. Paik and T. Hyeon, *J. Am. Chem. Soc.*, 2006, **128**, 10658–10659.

7 L. Y. Zhang, X. J. Zhu, D. J. Jiao, Y. L. Sun and H. W. Sun, *Mater. Sci. Eng., C*, 2013, **33**, 1989–1992.

8 Y. H. Wu, G. X. Chang, Y. B. Zhao and Y. Zhang, *J. Nanopart. Res.*, 2014, **16**, 8.

9 W. H. K. Kuo and H. A. Chase, *Biotechnol. Lett.*, 2011, **33**, 1075–1084.

10 C. Smith, *Nat. Methods*, 2005, **2**, 71–77.

11 G. Q. Jian, Y. X. Liu, X. W. He, L. X. Chen and Y. K. Zhang, *Nanoscale*, 2012, **4**, 6336–6342.

12 Y. T. Zhang, D. Li, M. Yu, W. F. Ma, J. Guo and C. C. Wang, *ACS Appl. Mater. Interfaces*, 2014, **6**, 8836–8844.

13 M. Zhang, X. W. He, L. X. Chen and Y. K. Zhang, *Nanotechnology*, 2011, **22**, 9.

14 S. Y. Huang and Y. C. Chen, *Anal. Chem.*, 2013, **85**, 3347–3354.

15 M. F. Shao, F. Y. Ning, J. W. Zhao, M. Wei, D. G. Evans and X. Duan, *J. Am. Chem. Soc.*, 2012, **134**, 1071–1077.

16 Z. Liu, M. Li, F. Pu, J. S. Ren, X. J. Yang and X. G. Qu, *J. Mater. Chem.*, 2012, **22**, 2935–2942.

17 J. Chun, S. W. Seo, G. Y. Jung and J. Lee, *J. Mater. Chem.*, 2011, **21**, 6713–6717.

18 Z. Liu, M. Li, X. J. Yang, M. L. Yin, J. S. Ren and X. G. Qu, *Biomaterials*, 2011, **32**, 4683–4690.

19 J. Lee, S. Y. Lee, S. H. Park, H. S. Lee, J. H. Lee, B. Y. Jeong, S. E. Park and J. H. Chang, *J. Mater. Chem. B*, 2013, **1**, 610–616.

20 J. N. Zheng, Z. Lin, W. Liu, L. Wang, S. Zhao, H. H. Yang and L. Zhang, *J. Mater. Chem. B*, 2014, **2**, 6207–6214.

21 Y. Wang, G. C. Wang, Y. Xiao, Y. L. Yang and R. K. Tang, *ACS Appl. Mater. Interfaces*, 2014, **6**, 19092–19099.

22 Y. T. Zhang, Y. K. Yang, W. F. Ma, J. Guo, Y. Lin and C. C. Wang, *ACS Appl. Mater. Interfaces*, 2013, **5**, 2626–2633.

23 Y. H. Wu, G. X. Chang, Y. B. Zhao and Y. Zhang, *Dalton Trans.*, 2014, **43**, 779–783.

24 S. W. Li, K. G. Yang, B. F. Zhao, X. Li, L. K. Liu, Y. B. Chen, L. H. Zhang and Y. K. Zhang, *J. Mater. Chem. B*, 2016, **4**, 1960–1967.

25 Y. Wang, J. He, J. W. Chen, L. B. Ren, B. W. Jiang and J. Zhao, *ACS Appl. Mater. Interfaces*, 2012, **4**, 2735–2742.

26 P. Krasucka, W. Stefaniak, A. Kierys and J. Goworek, *Microporous Mesoporous Mater.*, 2016, **221**, 14–22.

27 J. He, C. L. Yang, X. H. Xiong and B. W. Jiang, *J. Polym. Sci., Part A: Polym. Chem.*, 2012, **50**, 2889–2897.

28 T. A. Vereshchagina, M. A. Fedorchak, O. M. Sharonova, E. V. Fomenko, N. N. Shishkina, A. M. Zhizhaev, A. N. Kudryavtsev, L. A. Frank and A. G. Anshits, *Dalton Trans.*, 2016, **45**, 1582–1592.

29 J. Z. Wang, A. Sugawara-Narutaki, M. Fukao, T. Yokoi, A. Shimojima and T. Okubo, *ACS Appl. Mater. Interfaces*, 2011, **3**, 1538–1544.

30 D. Tsiourvas, A. Tsetsekou, A. Papavasiliou, M. Arkas and N. Boukos, *Microporous Mesoporous Mater.*, 2013, **175**, 59–66.

31 K. Salimi, D. D. Usta, O. Celikbicak, A. Pinar, B. Salih and A. Tuncel, *Colloids Surf., B*, 2017, in revision.

32 B. Elmas, M. Tuncel, G. Yalcin, S. Senel and A. Tuncel, *Colloids Surf., A*, 2005, **269**, 125–134.

33 C. Kip, B. Maras, O. Evirgen and A. Tuncel, *Colloid Polym. Sci.*, 2014, **292**, 219–228.

34 A. Tuncel, *J. Appl. Polym. Sci.*, 1999, **71**, 2291–2302.

35 D. D. Usta, K. Salimi, A. Pinar, I. Coban, T. Tekinay and A. Tuncel, *ACS Appl. Mater. Interfaces*, 2016, **8**, 11934–11944.

36 Z. Y. Ma, D. Dosev and I. M. Kennedy, *Nanotechnology*, 2009, **20**, 085608.

37 Z. Yıldırım and E. Çelik, *J. Chem. Technol. Biotechnol.*, 2017, **92**, 319–324.

38 Z. Y. Ma, Y. P. Guan and H. Z. Liu, *J. Polym. Sci., Part A: Polym. Chem.*, 2005, **43**, 3433–3439.

39 Y. Zhang, M. Zhang, J. Yang, L. Ding, J. Zheng, J. Xu and S. Xiong, *Nanoscale*, 2016, **8**, 15978–15988.

40 A. A. Khassin, T. M. Yurieva, M. P. Demeshkina, G. N. Kustova, I. S. Itenberg, V. V. Kaichev, L. M. Plyasova, V. F. Anufrienko, I. Y. Molina, T. V. Larina, N. A. Baronskaya and V. N. Parmon, *Phys. Chem. Chem. Phys.*, 2003, **5**, 4025–4031.

41 W. F. Ma, Y. Zhang, L. L. Li, Y. T. Zhang, M. Yu, J. Guo, H. J. Lu and C. C. Wang, *Adv. Funct. Mater.*, 2013, **23**, 107–115.

42 Z. Rashid, H. Naeimi, A. H. Zarnani, M. Nazari, M. R. Nejadmoghaddam and R. Ghahremanzadeh, *RSC Adv.*, 2016, **6**, 36840–36848.

43 X. Y. Qi, L. Chen, C. Q. Zhang, X. Y. Xu, Y. D. Zhang, Y. Bai and H. W. Liu, *ACS Appl. Mater. Interfaces*, 2016, **8**, 18675–18683.